Nano Energy 31 (2017) 152–159

Contents lists available at ScienceDirect

Nano Energy

journal homepage: www.elsevier.com/locate/nanoen

Nano-micro-porous skutterudites with 100% enhancement in ZT for high performance thermoelectricity

Atta U. Khan[a], Kazuaki Kobayashi[a], Dai-Ming Tang[a], Yusuke Yamauchi[a], Kotone Hasegawa[a], Masanori Mitome[a], Yanming Xue[a], Baozhen Jiang[b], Koichi Tsuchiya[b,c], Dmitri Golberg[a,c], Yoshio Bando[a], Takao Mori[a,c,*]

[a] National Institute for Materials Science (NIMS), International Center for Materials Nanoarchitechtonics (MANA), Namiki 1-1, Tsukuba 305-0044, Japan
[b] National Institute for Materials Science (NIMS), Research Center for Structural Materials, Sengen 1-2-1, Tsukuba 305-0047, Japan
[c] University of Tsukuba, Graduate School of Pure and Applied Sciences, 1-1-1 Tennoudai, Tsukuba 305-8671, Japan

ARTICLE INFO

Keywords:
Energy conversion
Materials science
Semiconductors
Solid-state chemistry
Thermoelectric materials

ABSTRACT

Increasing energy demands require new materials, e.g., thermoelectrics, for efficient energy conversion of fossil fuels. However, their low figure of merit (ZT) limits widespread applications. Nanostructuring has been an effective way of lowering the thermal conductivity. However, grain growth at elevated temperature is still a big concern, for otherwise expected to be long-lasting thermoelectric generators. Here, we report a porous architecture containing nano- to micrometer size irregularly shaped and randomly oriented pores, scattering a wide spectrum of phonons without employing the conventional rattling phenomenon. Lattice thermal conductivity reaches the phonon glass limit. This design yields & $2gt;100% enhancement in ZT, as compared to the pristine sample. An unprecedented and very promising ZT of 1.6 is obtained for Co23.4Sb69.1Si1.5Te6.0 alloy, by far the highest ZT ever reported for un-filled skutterudites, with further benefits, i.e. rare-earth-free and improved oxidation resistance enabling simple processing.

1. Introduction

Thermoelectric materials have many potential applications, e.g. for electricity production in deep space, in military equipment and mainly for waste heat recovery from different sources, e.g. power plants, automobiles etc. [1,2]. However, their relatively low conversion efficiency, which is a function of the dimensionless figure of merit (ZT) $=\alpha^2\sigma T/\kappa$ (α is the Seebeck coefficient, σ electrical conductivity, T absolute temperature, and κ the total thermal conductivity [3]) hinders their widespread applications. The highest ZT reported in bulk thermoelectric materials (PbTe) is 2.2 [4], while recently, in a single crystal (SnSe), a ZT as high as 2.6 in one dimension was reported [5]. However, extreme toxicity of Pb along with large amount of expensive Te in the case of PbTe, and anisotropy of SnSe may question their feasibility for applications on large scale.

Band structure engineering has helped researchers in optimizing the power factor ($\sigma\alpha^2$) [6]. For high efficiency, high power factor with low thermal conductivity is essential. Phonon Glass Electron Crystal approach (PGEC) [7] was extensively studied in the recent past, to obtain high ZT thermoelectrics. According to Wiedemann-Franz relationship, thermal conductivity consists of two components, (1) electronic contribution due to electrons flow, which is proportional to the electrical conductivity, and (2) lattice thermal conductivity caused by lattice vibrations called phonons. Based on electron crystal concept, the electronic part (can only be decreased by a deterioration in electrical conductivity) should be preserved. So it is merely the phononic part that can potentially be reduced. Traditionally, four major ways are employed to diminish the lattice thermal conductivity, the first two being, (a) nanostructuring to increase the phonon scattering from the grain boundaries; (b) insertion of point defects through alloying; and (c) precipitation of secondary phases in the matrix to scatter phonons from the fine grains of secondary phases. Nanostructuring is generally only feasible for low temperatures, owing to tendency of grain growth at high temperatures. On the other hand, precipitation of secondary phases affects primarily high-frequency phonons but low-frequency phonons in heat transport remain unaffected [8]. Point defect scatter-

Abbreviations: ZT, Figure of Merit; PGEC, Phonon Glass Electron Crystal; CIP, Cold Isostatic Press; XRD, X-ray Diffraction; SPS, Spark Plasma Sintering; DSC, Differential Scanning Calorimetry; Cp, Heat Capacity; SEM, Scanning Electron Microscope; LDA, Local Density Approximation; BH, von Barth-Hedin; DOS, Density Of States; EDX, Energy Dispersive X-ray; RE, Rare Earth

* Corresponding author at: National Institute for Materials Science (NIMS), International Center for Materials Nanoarchitechtonics (MANA), Namiki 1-1, Tsukuba 305-0044, Japan.
E-mail address: MORI.Takao@nims.go.jp (T. Mori).

http://dx.doi.org/10.1016/j.nanoen.2016.11.016
Received 5 July 2016; Received in revised form 7 November 2016; Accepted 9 November 2016
Available online 12 November 2016

ing is generally more effective if an element with considerable atomic size difference is inserted, leading to limited options. The third approach, which is limited to cage compounds, (d) filling-rattling phenomenon is frequently manipulated to reduce thermal conductivity but filling atoms often comprise rare-earth elements which are expensive (although mischmetal has been pointed out as a cost saving alternative [9]), or being extremely air-sensitive, such as barium [9–14]. Although, the exact role of filler atoms has been controversial [15], there have been many reports on multi-filled skutterudites [9–13,13,14,14–19]. Despite the fact that high ZT is reported in rare earths-filled skutterudites [9–19], the presence of rare earths elements in only certain areas of the world, hamper their widespread use and demand finding a better way of lowering their thermal conductivity. Porosity has been widely used to lower the thermal conductivity of materials, where electrical conductivity is not a concern. However, in thermoelectrics, degradation of electrical conductivity with increasing porosity is a major drawback. Meanwhile, it has been proved that the porous nano-structures, having controlled porosity [20–23] possess a very low thermal conductivity, along with good power factor. However, initial attempts in past to utilize porosity, to lower the thermal conductivity and to enhance the ZT of skutterudites, failed [24]. Although, porosity effectively lowered the thermal conductivity, it was counterbalanced by the degradation in electrical conductivity, resulting in no net improvement of ZT. Moreover, porosity is reported to greatly enhance the Seebeck coefficient [25,26] but no such thing was observed in the current study.

We report here, Si and Te co-doped bulk porous un-filled skutterudites producing a very attractive ZT of 1.6. This porous bulk architecture contains nano- to micrometer size pores. Pore size of this range seems to effectively interact with relatively long mean path phonons, reported to be responsible for heat conduction in $CoSb_3$ [27]. These all-scale, irregular, randomly oriented pores effectively scatter a wide spectrum of phonon. In previous attempts, sintering under low pressure was applied, to obtain porous skutterudites [24]. This methodology resulted in poor densification in all areas of samples. In the present study, due to different approach to obtain porosity, we have random distribution of pores, along with very dense areas distributed in the whole sample. Combination of these two, allows the electrons having short mean free path, to move freely, while interrupting the phonons travel, having rather long mean free paths, converting the material into a porous “phonon glass electron crystal (PGEC)” [7] bulk structure. It resulted in a drastic decline of lattice thermal conductivity with moderate degradation of power factor, giving rise to a & $2gt;100% increase in ZT (Fig. 1(a-d)), comparable to the multi-filled skutterudites [9–19] and far higher than the highest values reported for unfilled skutterudites [28–30].

2. Materials and methods

Samples were prepared by sealing stoichiometric amounts of high purity elemental powders (1–2% additional Sb was added). Details about the composition of the prepared samples are given in Supplementary material Table S1. These powders were sealed in quartz under vacuum and were heated to 1050 °C for 5 h, furnace cooled to 800 °C, kept for 2 h, further cooled down to 600 °C and kept there for 15 h, followed by cooling to room temperature. Samples were then ground in a SiC mortar in air, pressed in a Cold Isostatic Press (CIP), sealed again in quartz under vacuum and the heating cycle mentioned above was repeated. Resulting samples were ground again without inert environment, and Powder X-ray Diffraction (XRD) was conducted by utilizing Cu Kα radiations, then the samples were sintered using Spark Plasma Sintering (SPS) at 600 °C for 5 min. Thermal diffusivity of these pellets was measured with a Laser Flash ULVAC-TC7000 instrument. Pellets were cut into rectangular shapes to run on an ULVAC-ZEM-5 apparatus for electrical resistivity and Seebeck coefficient measurements simultaneously. Differential Scanning Calorimetry (DSC-8231, Thermo Plus Evo2, Rigaku) was employed to measure the specific heat capacity (Cp). Thermal conductivity was calculated as a product of thermal diffusivity*density*Cp. A Scanning Electron Microscope (SEM, S-4800, Hitachi) was utilized for microstructure characterization.

All the samples had a density of ≥94% of the theoretical density after sintering but before annealing. Two different pellets from the same sample powder were sintered; one of these was used to measure all the properties, while the 2nd pellet was sealed in a quartz tube under vacuum and annealed at 600 °C for 15 h, followed by cooling to room temperature. These pellets, however, had a lower density (around 88% of the theoretical density). After grinding all the surfaces of the pellets, these were employed for thermoelectric properties measurements in the same way as for other pellets.

The pore size distribution of $CoSb_{2.75}Si_{0.075}Te_{0.175}$ was obtained by mercury intrusion porosimetry (Micromeritics AutoPore IV 9520). Vickers microhardness measurement was carried out with an applied load of 0.98 N for 15 s (AMT-X7FS, Matsuzawa).

2.1. Calculations

The present total energy pseudopotential calculations [31–33] were based on local density approximation (LDA) in the density functional theory [34,35] (DFT) with the von-Barth and Hedin (BH) interpolation formula [36] for the exchange-correlation. Cubic structures were kept in the structural relaxation for most cases. Their lattice constants and internal atom positions were structurally relaxed. Although, there are many possible combinations of replaced atom positions for Si and Te in all calculated compounds, we chose only a few combinations for each compound.

3. Results and discussion

Si and Te doped samples were synthesized by reacting high purity elements followed by a solid state reaction. Obtained ingots were pulverized and sintered by utilizing spark plasma sintering (SPS) which yielded dense pellets (for density, please see Supplementary material Table S1). The temperature-dependent thermal and electrical transport properties are summarized in Supplementary material Fig. S2. The general trend was similar to that reported for Te doping [28–30], showing an increasing trend of ZT with rising Te content, mainly due to the enhancement in electrical conductivity and Seebeck coefficient, with Si addition having a less pronounced but positive effect on ZT (for details, please see Supplementary material text and Fig. S2).

Careful annealing of the samples yielded striking results with respect to the thermal properties. Newly sintered pellets, sealed in quartz tubes under vacuum were annealed for 15 h at 600 °C. As shown in Fig. 2c for $CoSb_{2.75}Si_{0.075}Te_{0.175}$ for example, an enormous drop in thermal conductivity was obtained when comparing the pristine sample with the annealed sample (the other samples will be discussed later), with only a petty degradation of electrical conductivity, which indicates that the decrease in thermal conductivity is predominated by lattice thermal conductivity (based on the Wiedemann-Franz relationship, with Lorentz number (Fig. S3, supplementary material) calculated from the observed Seebeck coefficient). To analyze the reason behind this drop in lattice thermal conductivity, we employed a scanning electron microscope (SEM) (Fig. 3a–d). A detailed study conducted on various samples, denoted the formation of irregular, randomly oriented, and altering sized pores after annealing. Micrographs of $CoSb_{2.75}Si_{0.075}Te_{0.175}$ sample clearly display the tiny pores of varying shapes and sizes (tens of nm to few micrometers), formed in the material after annealing (Fig. 3b and c), while almost no pores are present in the pristine sample (Fig. 3a). The formation of pores is also obvious from the decay in density after annealing (Supplementary material Table S1). Moreover, no porosity increase was observed in Te free samples after annealing (Fig. 3d), pointing towards the role of Te

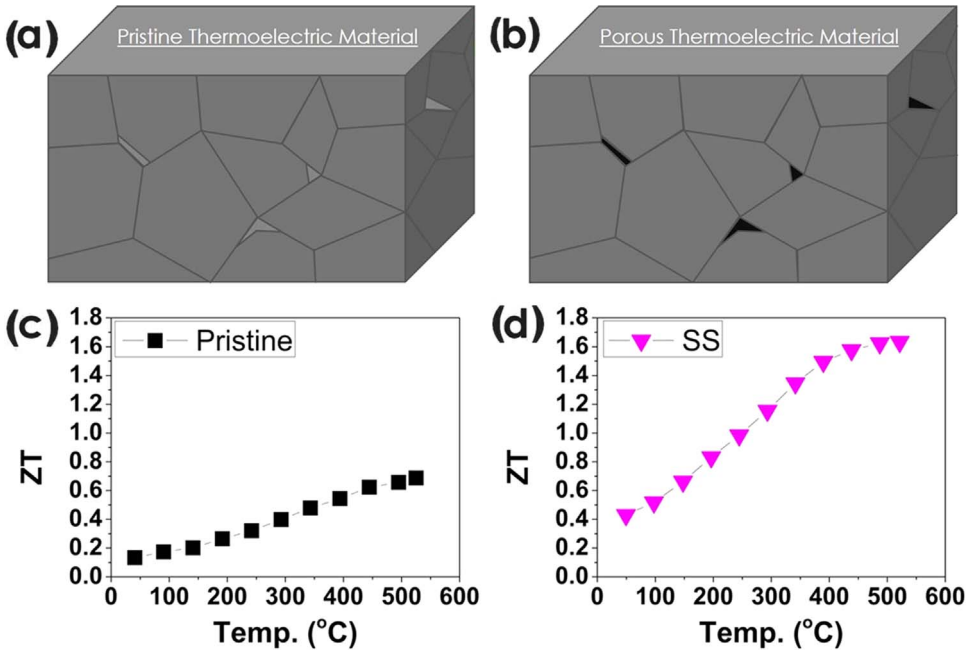

Fig. 1. Schematic illustration of porosity and its effect on ZT. (a) A compact block representative of the pristine sample, with grains of the secondary phase in light color and (b) block with pores, formed due to evaporation of secondary phase, having random, irregular and varying sized pores (black areas). (c) ZT around 0.7 is obtained for the pristine samples, without pores. (d) Porosity effect gives rise to a high ZT showing more than 100% increase as compared to the pristine sample.

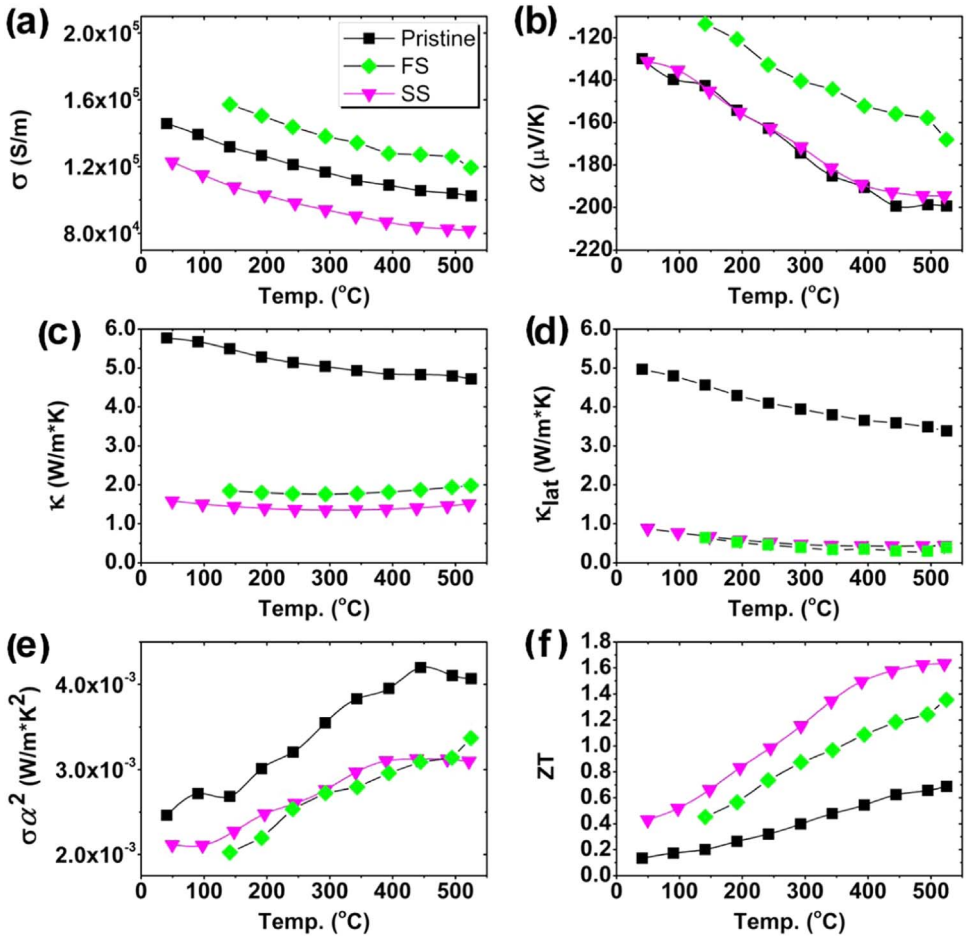

Fig. 2. Temperature-dependent thermoelectric properties of selected samples are presented, indicating the role of porosity in decreasing lattice thermal conductivity and thereby, enhancing ZT. "Pristine ($CoSb_{2.75}Si_{0.075}Te_{0.175}$)" represents the sample prior to annealing. First sample synthesized during the phase diagram study, is represented by FS ($Co_{23}Sb_{67}Te_{10}$, at%) and SS ($Co_{23.4}Sb_{69.1}Si_{1.5}Te_6$, at%) is the sample with high ZT. Symbol notation remains the same in all panels. (a) Electrical conductivity (σ), (b) Seebeck coefficient (α), (c) total thermal conductivity (κ), (d) lattice thermal conductivity (κ_{lat}), (e) power factor ($\sigma\alpha^2$) and (f) ZT.

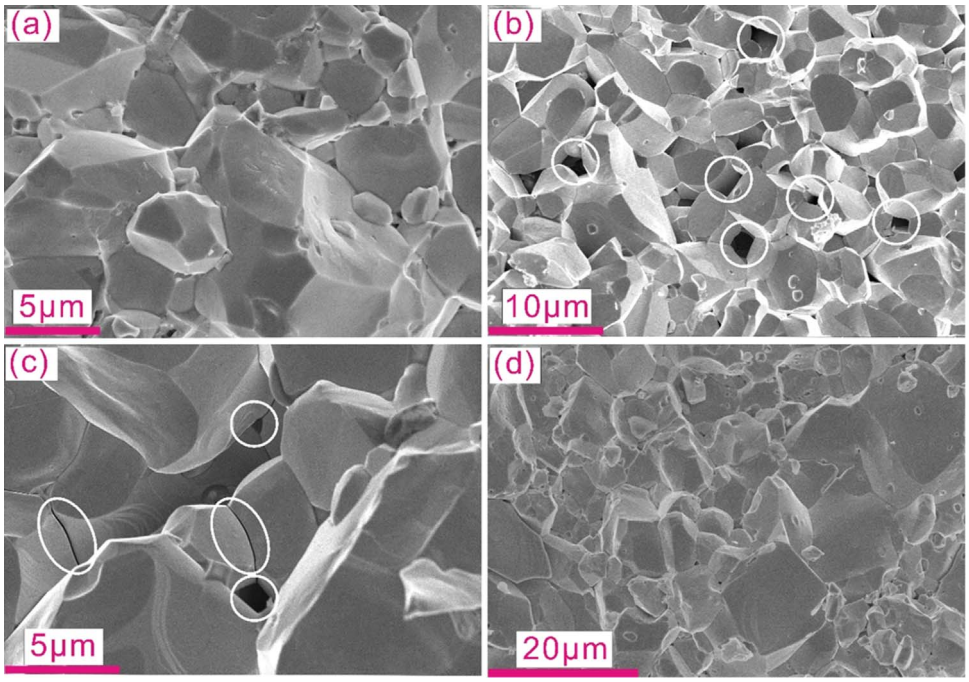

Fig. 3. SEM micrographs of different samples before and after annealing. Cracked surface of $CoSb_{2.75}Si_{0.075}Te_{0.175}$ sample (a) prior to annealing, also named as "pristine", and (b) after annealing, white circles mark the pores in the materials. (c) Nanometer-scale pores along grain boundaries are observed in addition to micrometer-sized pores, while (d) indicates the absence of free Si and/or pores in $CoSb_{2.875}Si_{0.125}$ after annealing.

containing phase in porosity enhancement. These micrographs also indicate moderate grain growth during annealing. Interestingly, the particles after annealing seem to be more regular and round as compared to the irregular ones before annealing, pointing towards improved crystallization after annealing, as expected. SEM micrographs gave a hint that the route cause behind this remarkable drop of thermal conductivity is the appearance of these tiny pores.

To have a proper insight into the size distribution of pores in the sample, we used mercury intrusion porosimetry. Average size of pores measured by this technique indicated that the majority of pores present are 500 nm in size (Supplementary material Fig. S4a), although there is a continuous peak starting from ~150 to 500 nm. This variation in size is in agreement with the size variation observed under SEM observations and proves the assumption of size variation. In contrast, the pristine sample shows no significant peak in the pore size distribution curve (Supplementary material Fig. S4(b)), showing no evidence of significant pores. The absence of the pores is also confirmed by SEM images (Fig. 3a).

Initial rough estimation of the effective thermal conductivity of porous structures by utilizing Eucken [37] model (although, this model is applicable to round and same size pores only), could not justify the enormous decline of thermal conductivity observed in the current study, as follows from a formula:

$$\kappa_{eff} \approx \kappa_m[2(1-\phi)/(2+\phi)] \quad (1)$$

where ϕ is the porosity, κ_m is the bulk thermal conductivity. If we consider 8% increase in porosity after annealing in our samples (based on the density difference before and after annealing, Table S1, Supplementary material), by using this equation, the estimated plunge in thermal conductivity should be around 12%, but it is much higher than that.

It is already reported that the average group velocities and density of states (DOS) of phonons are suppressed in case of holey structures at low temperatures and this suppression is expected to intensify as the temperature increases [20,21]. It is also proclaimed that imperfections in pores packing could potentially introduce additional phonon scattering [22]. A sizeable fraction of heat transfer is carried out by relatively long mean free path phonons at room temperature [8]. Acoustic phonons generally possess longer mean free paths, as compared to optical phonons in $CoSb_3$ [27] and they reach ~500 nm for low frequency phonons at room temperature. Additionally, it has been shown that alloying significantly raises the fraction of heat carried by long-wavelength phonons due to mass-difference scattering, efficiently blocking high-frequency phonons [38]. We can expect a similar effect in the material under investigation, as $CoSb_3$ was alloyed by Te and Si. So even bigger size pores may play a significant role in reducing the lattice thermal conductivity by targeting long-wavelength phonon scattering. Combination of micro- and nanometer sized pores can scatter wide range of diverse frequency phonons. Furthermore, pores of different shapes will scatter phonons in different directions, giving rise to diffusive scattering, which is also considered helpful in reducing the lattice thermal conductivity.

Moreover, it is expected that the improved crystallization due to annealing, should generate smoother grain surfaces, as can be observed in Fig. 3b. These smooth surfaces can reflect the phonons in a purely specular way (at least some surfaces). Reflected waves have the possibility to cause wave interference resulting in reduced group velocities and thus, low thermal conductivity [23,39]. Although, this contribution is likely minor, combination of all above-mentioned phenomena will strongly affect the phonon mean free path and will shorten it to a great extent. Subsequently, lattice thermal conductivity would face a massive drop and our results agree well with such an assumption.

Consequently, $CoSb_{2.75}Si_{0.075}Te_{0.175}$ shows high porosity and a big drop in thermal conductivity. Actually the thermal conductivity of $CoSb_{2.75}Si_{0.075}Te_{0.175}$ (~1.4 W/m K) is even lower than that for the rare-earth triple-filled skutterudites [10], with lattice thermal conductivity being less than ~0.9 W/m K at 50 °C. It is even lower than vitreous silica and slightly higher than the theoretically calculated minimum lattice thermal conductivity of filled skutterudites (~0.7 W/m K) [40], reaching phonon glass limit for $CoSb_3$. According to our best knowledge, this is one of the lowest lattice and total thermal conductivity ever reported for all skutterudites having a power factor higher than 3 mW/m K^2.

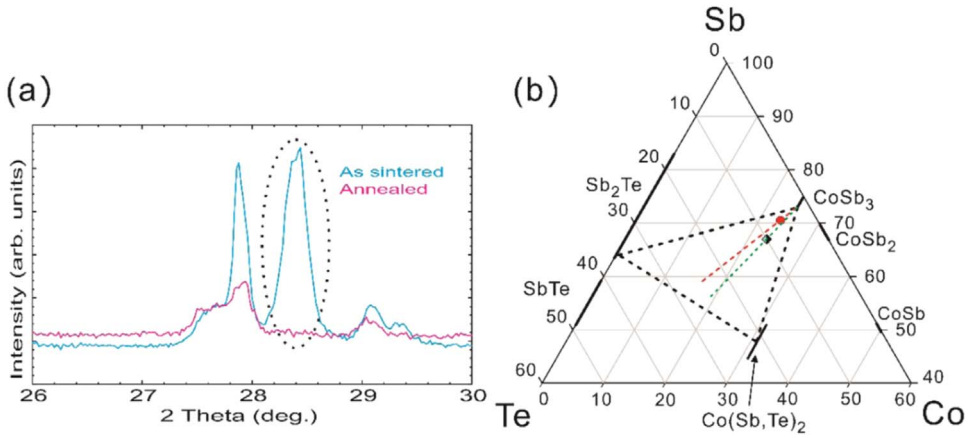

Fig. 4. XRD and phase diagram. (a) XRD of $Co_{23.4}Sb_{69.1}Si_{1.5}Te_6$ (at%, named as SS) as sintered and annealed pellets. Dotted circle highlights the main peak of Sb_2Te phase, which completely disappeared after annealing. (b) Tentative partial phase diagram of Co-Sb-Te system at 600 °C. Diamond symbol denotes the sample FS ($Co_{23}Sb_{67}Te_{10}$, at%) and red circle represents SS sample ($Co_{23.4}Sb_{70.6}Te_6$, at%. Although, 1.5 at% Sb was replaced by Si in this sample, but for the sack of simplicity, we show only 3 elements here). Green and red dotted lines serve as an eye guide to estimate the amount of secondary phase/s in the sample. It is obvious that SS involves less amount of $Co(Sb,Te)_2$ phase as compared to FS. $Co(Sb,Te)_2$ phase is metallic and its large amounts should be avoided to achieve high ZT.

We were able to elucidate the origin of creation of these remarkably effective pores. X-ray diffraction (XRD) of the sintered pellets, prior to and after annealing, served the purpose. We observed a small peak before annealing, which vanished after annealing. The intensity of this peak was very low. Therefore, XRD was carried out for a selected small range $26 \leq 2\theta \leq 30$ (deg.) (Fig. 4a) in order to solely focus on that peak. It can unambiguously be seen that the peak at $2\theta = 28.4$ (deg.), present prior to annealing, completely disappears after annealing. This is the highest intensity peak of Sb_2Te. Moreover, Energy Dispersive X-ray (EDX) mapping, indicated the presence of Sb_2Te phase (Supplementary material Fig. S5a–d) on the grain boundaries. No such phase after annealing was observed, providing additional evidence that Sb_2Te is the sole responsible phase for pores formation.

Inspired by the general considerable enhancement in ZT after annealing (Fig. 2 and Supplementary material Fig. S2), we decided to get further insights from a phase diagram study (Fig. 4b). Such kind of approach has already been proved useful in optimizing the ZT of Ce-filled skutterudites [41]. Primary purpose of phase diagram-aided study in our case was to optimize a composition which could make the results repeatable without precipitating too much of the secondary phases and to confirm the role of Sb_2Te phase for the formation of pores. A phase diagram targeted a new sample with nominal composition $Co_{23.0}Sb_{67.0}Te_{10.0}$. This was first synthesized (labelled as "first synthesis" FS) and showed an enhancement in ZT, although, it had no Si in it. Absence of Si helped us to reliably conclude that Si had no role in pores emergence. During sintering, some melt appeared outside the die, which was collected and characterized; it was confirmed to be Sb_2Te phase. This phase starts to melt at around 500 °C and due to high pressure, most of the phase is squeezed out. However, sintered pellets always have a small amount of fine pores, and it can be expected that a part of the Sb_2Te remained and solidified on cooling, since we detected that the pristine sample actually had a small amount of this phase (Fig. 4a). During annealing under vacuum at high temperature (higher than the melting point of this phase), Sb_2Te evaporated and during its escape, it likely paved small pores in the sample, mainly at grain boundaries, as typically observed by SEM (Fig. 3b,c). In the case of $Co_{23.0}Sb_{67.0}Te_{10.0}$, although, this sample had a good electrical conductivity over the entire temperature range (Fig. 2a), it showed a low Seebeck coefficient (Fig. 2b). This can be explained by the relatively large amounts of metallic $Co(Sb,Te)_2$ secondary phase. Thermal conductivity of $Co_{23.0}Sb_{67.0}Te_{10.0}$ was low but not as low as for the high ZT samples (Fig. 2c) and showed an increase at elevated temperatures, most probably due to the bipolar effect, arising from thermal excitation of minority charge carriers [42]. In order to enhance the Seebeck coefficients and to suppress the bipolar effect, by studying the phase diagram, we shifted the composition towards the Sb-rich area (Fig. 4b). Furthermore, we added a small amount of Si which already had been part of the high ZT samples. A sample with nominal composition $Co_{23.4}Sb_{69.1}Si_{1.5}Te_{6.0}$ was thus synthesized. Although its power factor remained the same (Fig. 2e), its Seebeck coefficient enhanced, as compared to $Co_{23.0}Sb_{67.0}Te_{10.0}$, and the bipolar effect suppressed, giving rise to a similar and repeatable very high ZT~1.6 (Fig. 4f), as was achieved already.

Thanks to the porous structures formed by annealing and their effect on the thermal conductivity, there has been an improvement of more than 100% in $Co_{23.4}Sb_{69.1}Si_{1.5}Te_{6.0}$, reaching a striking ZT of 1.6 at around 500 °C, despite the absence of rattling rare-earth atoms. It makes it a very promising approach for thermoelectric applications, especially in cases where heavy dependence on the rare earth (RE) elements should be avoided. We were also able to process the material in air and stored it in ambient environment, without relying on a glovebox which is another major advantage compared to rare earth or alkaline metals containing skutterudites.

4. Calculations

To theoretically understand the effect of Si and Te doping, we calculated the band structures with different Si and Te contents. As a result of structural relaxation for the $Co_4Sb_{10}Si_1Te_1$, $Co_8Sb_{23}Te_1$, $Co_8Sb_{23}Si_1$, $Co_8Sb_{22}Si_2$, $Co_8Sb_{22}Si_1Te_1$, $Co_8Sb_{21}Si_1Te_2$, and $Co_8Sb_{21}Si_2Te_1$ structures, their volumes decrease in comparison to that of Co_4Sb_{12} (skutterudite) with the exception of $Co_8Sb_{23}Te_1$. The volume of $Co_8Sb_{21}Si_2Te_1$ is slightly smaller than that of Co_4Sb_{12} but its difference is negligible. We qualitatively obtained results where a smaller Si-Te distance is energetically more favorable than a longer case in $Co_4Sb_{10}Si_1Te_1$ and $Co_8Sb_{22}Si_1Te_1$. This implies that the replaced Si and Te atoms create co-doped pairs. All electronic band structures were calculated by LDA(BH) for Co_4Sb_{12}, $Co_4Sb_{10}Si_1Te_1$, and $Co_8Sb_{22}Si_1Te_1$, and these showed semiconducting natures in accordance with the experimental results. The density of states (DOS) of $Co_8Sb_{22}Si_1Te_1$, $Co_8Sb_{21}Si_1Te_2$, and $Co_8Sb_{21}Si_2Te_1$ are denoted in Fig. 5a, b, and c, respectively, with their band gaps indicated by "0" on the vertical line. From Fig. 5a, it is obvious that $Co_8Sb_{22}Si_1Te_1$ is semiconducting. In contrast, $Co_8Sb_{21}Si_1Te_2$ and $Co_8Sb_{21}Si_2Te_1$ are metallic, as exhibited in Fig. 5b and c, these findings also agree well with the experimental data (Supplementary material Fig. S2). The electronic states of $Co_8Sb_{23}Te_1$ (not shown) and $Co_8Sb_{23}Si_1$ (see inset in Fig. 5c) are also metallic (see Supplementary

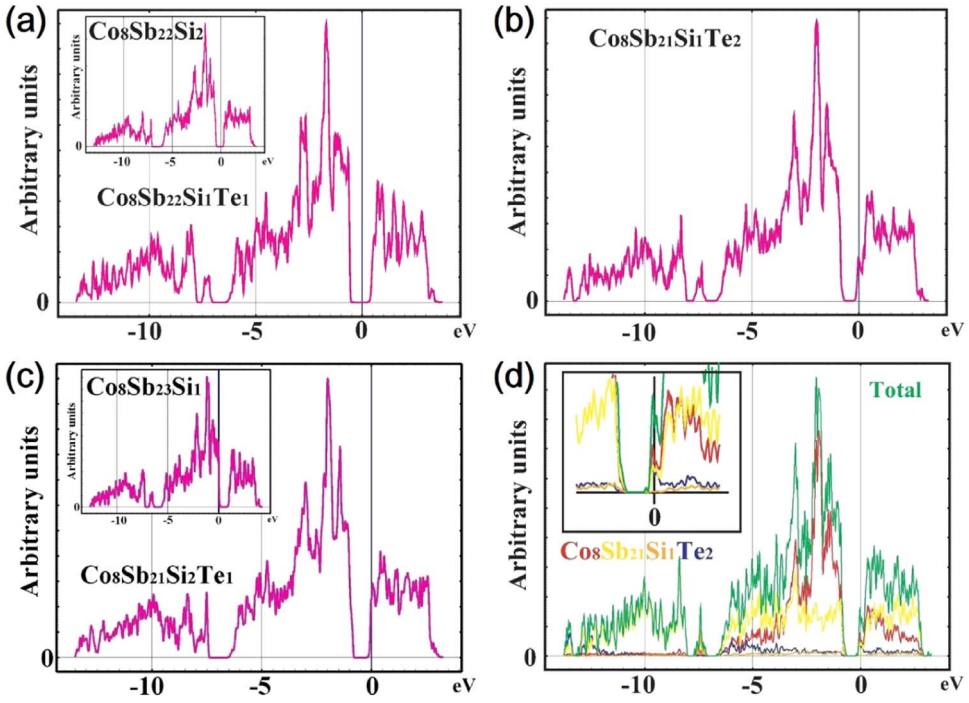

Fig. 5. The density of states (DOS) of (a) $Co_8Sb_{22}Si_1Te_1$ ($Co_8Sb_{22}Si_2$ as an inset), (b) $Co_8Sb_{21}Si_1Te_2$, (c) $Co_8Sb_{21}Si_2Te_1$ ($Co_8Sb_{23}Si_1$ as an inset) and (d) the total and partial DOS of $Co_8Sb_{21}Si_1Te_2$ (expanded DOS around the Fermi level as the inset) are drawn, respectively. The Fermi level is indicated by "0"' on the vertical line in the DOS curves. Total DOS of $Co_8Sb_{21}Si_1Te_2$ and partial DOS of Co, Te, Sb, and Si are indicated by green, red, blue, yellow, and orange curves, respectively. In the inset of expanded DOS, the yellow line (Sb) around the Fermi level is denoted finer in order to see the blue line (Te).

material Table S2). The total numbers of valence electrons for $Co_8Sb_{23}Te_1$ and $Co_8Sb_{21}Si_1Te_2$ are one electron larger than those of $Co_8Sb_{22}Si_1Te_1$ and Co_8Sb_{24}. This leads to the one electron doping (like an n-type) for a semiconducting system and the system becomes metallic. On the other hand, the total numbers of valence electrons for $Co_8Sb_{23}Si_1$ and $Co_8Sb_{21}Si_2Te_1$ are one electron fewer than those of $Co_8Sb_{22}Si_1Te_1$ and Co_8Sb_{24}. Although, this leads to the one hole doping (like a p-type) for a semiconducting system, and the system becomes metallic, the electronic states of $Co_8Sb_{21}Si_2Te_1$ demonstrate an n-type status, as displayed in Fig. 5c. This trend is consistent with Seebeck coefficient behavior of $CoSb_{2.875}Si_{0.125}$ (p-type) and $CoSb_{2.75}Si_{0.175}Te_{0.075}$ (n-type) in Fig. S2d. We calculated $Co_8Sb_{22}Si_2$ (see Fig. 5a inset) in order to compare with $Co_8Sb_{21}Si_2Te_1$. The electronic state of $Co_8Sb_{22}Si_2$ is semiconducting. Although n-type behavior of $Co_8Sb_{21}Si_2Te_1$ seems to be unusual, the substitution of Te for Sb transfers the electronic states from semiconducting to metallic (one electron doping as n-type) in $Co_8Sb_{22}Si_2$. For $Co_8Sb_{21}Si_1Te_2$, total and partial DOS are shown in Fig. 5d. The largest contribution comes from Co in the range of −3.0 to 0.0 eV. In contrast, the partial DOS of Sb is distributed in the whole range. There is a finite DOS of Te at the Fermi level, although contributions of Te and Si are small as compared to Co and Sb.

In general, the values and behavior of the electrical conductivity and Seebeck coefficient (Fig. S2b and d) are consistent with the calculated DOS results as shown Fig. 5a–c because their curves around the valence band top, conduction band bottom, and Fermi level are similar to each other. From Fig. 5a to c and the inset of Fig. 5(d), each Fermi level is close to the sharp peak and the DOS curves at the Fermi level are quite sharp and distorted by Te (Fig. 5d) [43]. Sharp DOS curves and peaks are obtained by flat bands. There is a relatively large contribution of Te (blue line) similarly to Co (red) and Sb (yellow) as shown in the inset of Fig. 5d. These sharp and distorted DOS may enhance thermoelectric properties [44], which leads to large experimental ZT values as shown in Fig. 2f and Supplementary material Fig. S2j.

5. Conclusions

This report will open up new gates for other researchers to improve their materials by utilizing this technique. The key factor of this report is the absence of expensive rare earth (RE) or any air sensitive elements, like alkali or alkaline earth metals. This keeps the material cost low, makes the processing easy, allows the material to be stored in ambient conditions while still delivers a high ZT, and makes it feasible for bulk production.

Acknowledgements

A.U.K. and T.M. conceived and designed the study. A.U.K. fabricated the high-quality samples and carried out the transport property measurements. K.K. carried out theoretical calculations. Y.Y. evaluated the size of holes. D.M.T suggested to measure the XRD with selected short range 2θ to confirm the presence and disappearance of Sb_2Te phase. A.U.K. wrote the draft and T.M. performed the main revision on it, with input from all co-authors. All of the authors contributed to the interpretation of the data and discussion. T.M., A.U.K., K.K., D.M.T., M.M., D.G. acknowledge support from CREST, JST.

Appendix A. Supplementary material

Supplementary data associated with this article can be found in the online version at doi:10.1016/j.nanoen.2016.11.016.

References

[1] K. Koumoto, T. Mori, Thermoelectric Nanomaterials, Springer, Heidelberg, 2013
[2] L.E. Bell, Science 321 (2008) 1457–1461.
[3] A.F.Ioffe, Infosearch Ltd., London, 1957.
[4] K. Biswas, J.Q. He, I.D. Blum, C.I. Wu, T.P. Hogan, D.N. Seidman, V.P. Dravid, M.G. Kanatzidis, Nature 489 (2012) 414–418.
[5] L.-D. Zhao, S.-H. Lo, Y. Zhang, H. Sun, G. Tan, C. Uher, C. Wolverton, V.P. Dravid, M.G. Kanatzidis, Nature 508 (2014) 373–377.
[6] Y. Tang, Z.M. Gibbs, L.A. Agapito, G. Li, H.-S. Kim, M.B. Nardelli, S. Curtarolo, G.J. Snyder, Nat. Mater. 14 (2015) 1223–1228.

[7] G.A. Slack, in: Ed. D. M. Rowe, CRC, 1995 (Ch. 34).
[8] J.A. Johnson, A.A. Maznev, J. Cuffe, J.K. Eliason, A.J. Minnich, T. Kehoe, C.M.S. Torres, G. Chen, K.A. Nelson, Phys. Rev. Lett. 110 (2013) 025901.
[9] G. Rogl, A. Grytsiv, P. Rogl, E. Bauer, M. Hochenhofer, R. Anbalagan, R.C. Mallik, E. Schafler, Acta Mater. 76 (2014) 434–448.
[10] X. Shi, J. Yang, J.R. Salvador, M. Chi, J.Y. Cho, H. Wang, S. Bai, J. Yang, W. Zhang, L. Chen, J. Am. Chem. Soc. 133 (2011) 7837–7846.
[11] H. Li, X. Tang, Q. Zhang, C. Uher, Appl. Phys. Lett. 94 (2009) 102114.
[12] J. Yang, Q. Hao, H. Wang, Y.C. Lan, Q.Y. He, A. Minnich, D.Z. Wang, J.A. Harriman, V.M. Varki, M.S. Dresselhaus, G. Chen, Z.F. Ren, Phys. Rev. B 80 (2009) 115329.
[13] G. Rogl, A. Grytsiv, P. Rogl, N. Peranio, E. Bauer, M. Zehetbauer, O. Eibl, Acta Mater. 63 (2014) 30–43.
[14] G. Rogl, A. Grytsiv, K. Yubuta, S. Puchegger, E. Bauer, C. Raju, R.C. Mallik, P. Rogl, Acta Mater. 95 (2015) 201–211.
[15] M.M. Koza, M.R. Johnson, R. Viennois, H. Mutka, L. Girard, D. Ravot, Nat. Mater. 7 (2008) 805–810.
[16] Y. Qiu, J. Xing, X. Gao, L. Xi, X. Shi, H. Gu, L. Chen, J. Mater. Chem. A 2 (2014) 10952–10959.
[17] Y. Qiu, L. Xi, X. Shi, P. Qiu, W. Zhang, L. Chen, J.R. Salvador, J.Y. Cho, J. Yang, Yuan-chun Chien, Sinn-wen Chen, Y. Tang, G.J. Snyder, Adv. Funct. Mater. 23 (2013) 3194–3203.
[18] T. He, J. Chen, H.D. Rosenfeld, M.A. Subramanian, Chem. Mater. 18 (2006) 759–762.
[19] W. Liu, X. Yan, G. Chen, Z. Ren, Nano Energy 1 (2012) 42–56.
[20] N. Zen, T.A. Puurtinen, T.J. Isotalo, S. Chaudhuri, I.J. Maasilta, Nat. Commun. 5 (3435) (2014) 1–9.
[21] J.-K. Yu, M. Slobodan, D. Tham, J. Varghese, J.R. Heath, Nat. Nanotechnol. 5 (2010) 718–721.
[22] J. Tang, H.-T. Wang, D.H. Lee, M. Fardy, Z. Huo, T.P. Russell, P. Yang, Nano Lett. 10 (2010) 4279–4283.
[23] P.E. Hopkins, C.M. Reinke, M.F. Su, R.H. Olsson III, E.A. Shaner, Z.C. Leseman, J.R. Serrano, L.M. Phinney, I. El-Kady, Nano Lett. 11 (2011) 107–112.
[24] L. Yang, J.S. Wu, L.T. Zhang, J. Alloy. Compd. 364 (2004) 83–88.
[25] Q. He, S. Hu, X. Tang, Y. Lan, J. Yang, X. Wang, Z. Ren, Q. Hao, G. Chen, Appl. Phys. Lett. 93 (2008) 042108.
[26] K. Koumoto, W.S. Seo, S. Ozawa, Appl. Phys. Lett. 71 (11) (1997) 1475–1476.
[27] R. Guo, X. Wang, B. Huang, Sci. Rep. 5 (7806) (2015) 1–9.
[28] W.-S. Liu, B.-P. Zhang, J.-F. Li, H.-L. Zhang, L.-D. Zhao, J. Appl. Phys. 102 (2007) 103717.
[29] T. Liang, X. Su, Y. Yan, G. Zheng, Q. Zhang, H. Chi, X. Tang, C. Uher, J. Mater. Chem. A 2 (2014) 17914–17918.
[30] C. Stiewe, L. Bertini, M. Toprak, M. Christensen, D. Platzek, S. Williams, C. Gatti, E. Meuller, B.B. Iversen, M. Muhammed, M. Rowe, J. Appl. Phys. 97 (2005) 044317.
[31] G.B. Bachelet, D.R. Hamann, M. Schluter, Phys. Rev. B 26 (1982) 4199–4228.
[32] N. Troullier, J.L. Martins, Phys. Rev. B 43 (1991) 1993–2006.
[33] K. Kobayashi, Mater. Trans. 42 (2001) 2153–2156.
[34] P. Hohenberg, W. Kohn, Phys. Rev. 136 (1964) B864–B871.
[35] W. Kohn, L.J. Sham, Phys. Rev. 140 (1965) A1133–A1138.
[36] U. von Barth, L. Hedin, J. Phys. C 5 (1972) 1629–1642.
[37] (a) A. Eucken, Ceram. Abstr. 11 (1932) 576;
(b) A. Eucken, Ceram. Abstr. 12 (1933) 231.
[38] M. Maldovan, Phys. Rev. Lett. 110 (2013) 025902.
[39] M. Maldovan, Nat. Mater. 14 (2015) 667–674.
[40] B.C. Sales, Mater. Res. Soc. Bull. 23 (1998) 15–21.
[41] Y. Tang, R. Hanus, S.-W. Chen, G.J. Snyder, Nat. Commun. 6 (7584) (2015) 1–7.
[42] H.J. Wu, L.-D. Zhao, F.S. Zheng, D. Wu, Y.L. Pei, X. Tong, M.G. Kanatzidis, J.Q. He, Nat. Commun. 5 (4515) (2014) 1–9.
[43] J.P. Heremans, V. Jovovic, E.S. Toberer, A. Saramat, K. Kurosaki, A. Charoenphakdee, S. Yamanaka, G.J. Snyder, Science 321 (2008) 554–557.
[44] G.D. Mahan, J.O. Sofo, Proc. Natl. Acad. Sci. USA 93 (1996) 7436–7439.

Dr. Atta Ullah Khan received his PhD in Physical Chemistry in 2011 from the University of Vienna, Austria. He has worked for 3 years as a postdoctoral fellow in National Institute for Materials Science (NIMS), Japan. Currently, he is working as a postdoctoral fellow in Rutgers, The State University of New Jersey, USA. His research includes synthesis of Inorganic materials through solid state synthesis, thermoelectric materials, phase equilibria and crystallography.

Dr. Kazuaki Kobayashi is a permanent principal researcher at International Center forMaterials Nanoarchitectonics (MANA), National Institute for Materials Science (NIMS), Japan. He received his Ph.D. in Physics in 1991 from the University of Tokyo. He is one of the specialists of the electronic structure calculation baseon density functional theory, and his research interests is to search unknown materials and to obtain their electronic and structural properties using the total energy pseudopotential method.

Dr. Dai-Ming Tang received his Ph.D. in materials science in 2010 from the Institute of Metal Research (IMR), Chinese Academy of Sciences (CAS). Currently he is a permanent researcher &$2 MANA scientist at International Center for Materials Nanoarchitectonics (MANA), National Institute for Materials Science (NIMS), Japan. His research interest is to understand structure-properties relationship and design new materials at multi-scales.

Prof. Yusuke Yamauchi received his PhD in 2007 from Waseda University in Japan. After receiving his PhD, he joined the National Institute for Materials Science (NIMS) and started his own research group on 'Inorganic materials chemistry'. He has published more than 400 papers in international refereed journals. He concurrently serves as a visiting professor at several universities (Tianjin University, Waseda University, and University of Wollongong), and an associate editor of APL Materials published by the American Institute of Physics (AIP). His major research interest is tailored design of novel nanoporous materials with various shapes and compositions toward practical applications.

Dr. Kotone Hasegawa's main research interests are nano-science and nanotechnologyusing transmission electron microscope, especially crystal orientation mapping using precession of electron beam (ASTER or A-COM). She is also interested in scanning probe microscopy using FIB-milled sharp metal tipwhich is fabricated by her. She received her PhD in physics department of Tohoku Univ. in Japan and worked in Tohoku Univ. as a COE fellow and assistant professor for totally 4 years. Now she's working as a technical staff in NIMS,MANA- Nanotubes group.)

Dr. Masanori Mitome is a permanent senior researcher at the National Institute for Materials Science (NIMS), Japan. He received his Ph.D. in Materials Science from the Tokyo Institute of Technology. Before completing his doctorate he has worked in the Canon Research Center as a permanent researcher. In 1997 he joined the National Institute for Research in Inorganic Materials that was reorganized to NIMS in 2001. He is one of the specialists of transmission electron microscopy, and his research interests include crystal structure analysis for nanomaterials and metrology using electron beam technology.

Dr. Yanming Xue received his Ph. D. in Materials Physics and Chemistry in 2014 from the Institute of Materials Science and Engineering, Hebei University of Technology. Now he is a postdoctoral fellow of Prof. Dmitri Golberg's group (Nanotubes Group) at the National Institute for Materials Science (NIMS). His research interests include controlled synthesis and exploration of fundamental physical properties of inorganic functional nanomaterials as well as their promising applications in energy storage science and engineering fields. His current research topic is the controlled fabrication, novel properties and engineering applications of boron nitride nanotubes and nanosheets.

Dr. Baozhen Jiang received his Ph.D. in materials science and engineering in 2015 from University of Tsukuba, Japan. Currently he works as a postdoctoral fellow in National Institute for Materials Science (NIMS), Japan. His main research interest is to understand the processing-microstructure-mechanical properties relationship of metallic alloys and study the mechanical properties of steel corrosion products in reinforced concrete.

Prof. Koichi Tsuchiya is the Director of Research Center for Structural Materials in National Institute for Materials Science (NIMS). He is also the Deputy Director of International Center for Young Scientists (ICYS) and a Professor in the Graduate School of Pure and Applied Sciences in the University of Tsukuba. He obtained his Ph. D. in Materials Science and Engineering from Northwestern University in 1991, his Masters in Applied Physics in 1986 and his Bachelor in 1984, both from Hokkaido University. His research interests are in structure-property relationship in metallic structural and functional materials, such as, Ti alloys, steels, shape memory alloys, intermetallics and metallic glasses.

Prof. Dmitri Golberg obtained his PhD degree in 1990 from Institute for Ferrous Metallurgy in Moscow, and joined NIMS, Tsukuba, Japan, 5 years later. He is an author of more than 620 original papers (cited over 26500 times, H-index-86) and over 100 patents. He was awarded Tsukuba Prize and became a recipient of the Thomson Reuters Research Front Award for his research on 1D-nanomaterials. Currently he is a Group Leader and a Principal Investigator within WPI-MANA-NIMS, and a Professor of the University of Tsukuba. His research focuses on nanoscale material property studies in TEM.

Prof. Yoshio Bando received a Ph.D. degree at Osaka University in 1975 and joined the National Institute for Research in Inorganic Materials (at present National Institute for Materials Science, NIMS) the same year. He is a Fellow of NIMS and a Chief Operating Officer of International Center for Materials Nanoarchitectonics (WPI-MANA). From 1979 to 1981, he has been a visiting scientist at the Arizona State University, USA. He is now an adjunct member of the Science Council of Japan and also a Fellow of The American Ceramic Society. He served as Editor-in-chief of Journal of Electron Microscopy from 2008 to 2012. His current research concentrates on synthesis and property of novel inorganic 1D/2D nanomaterials and their in-situ TEM analysis.

Prof. Takao Mori, NIMS & $2 Univ. Tsukuba, Tsukuba, Japan. Email: MORI.Takao@nims.go.jp. Prof. Takao Mori's present research fields focus on Thermoelectrics, Magnetism, Solid State Physics, Inorganic Materials Science, and Material Synthesis. He is particularly interested in inorganic compounds with "network" structures; atomic clusters, cages, and nets. One particular focus is to develop thermoelectric materials viable for the first wide scale applications. From 2010 Prof. Mori has been a Visiting Professor at Hiroshima University , and Adj. Prof. at Univ. of Tsukuba. Prof. Mori is also Lab Director of the NIMS Open Innovation Center (NOIC), Thermal Energy Conversion Lab, which is a multi-company and institute open innovation endeavor carrying out challenging research on thermoelectrics and